

# Bandwidth-controlled Mott transition in $\kappa$ -(BEDT-TTF)<sub>2</sub>Cu[N(CN)<sub>2</sub>]Br<sub>x</sub>Cl<sub>1-x</sub>: Optical studies of localized charge excitations

Daniel Faltermeier, Jakob Barz, Michael Dumm, and Martin Dressel\*

*1. Physikalisches Institut, Universität Stuttgart, Pfaffenwaldring 57, 70550 Stuttgart, Germany*

Natalia Drichko

*1. Physikalisches Institut, Universität Stuttgart, Pfaffenwaldring 57, 70550 Stuttgart, Germany**and Ioffe Physico-Technical Institute, Russian Academy of Science, Politekhnicheskaya 26, 194021 St. Petersburg, Russia*

Boris Petrov, Victor Semkin, and Rema Vlasova

*Ioffe Physico-Technical Institute, Russian Academy of Science, Politekhnicheskaya 26, 194021 St. Petersburg, Russia*

Cécile Mezière and Patrick Batail

*Laboratoire CIMI, FRE 2447 CNRS-Université d'Angers, Bâtiment K, UFR Sciences, 2 Boulevard Lavoisier, 49045 Angers, France*

(Received 12 March 2007; revised manuscript received 3 June 2007; published 10 October 2007)

Infrared reflection measurements of the half-filled two-dimensional organic conductors  $\kappa$ -(BEDT-TTF)<sub>2</sub>Cu[N(CN)<sub>2</sub>]Br<sub>x</sub>Cl<sub>1-x</sub> [BEDT-TTF denotes bis-(ethylenedithio)tetrathiafulvalene] were performed as a function of temperature ( $5\text{ K} < T < 300\text{ K}$ ) and Br substitution ( $x=0\%$ ,  $40\%$ ,  $73\%$ ,  $85\%$ , and  $90\%$ ) in order to study the metal-insulator transition. We can distinguish absorption processes due to itinerant and localized charge carriers. The broad midinfrared absorption has two contributions: transitions between the two Hubbard bands and intradimer excitations from the charges localized on the (BEDT-TTF)<sub>2</sub> dimer. Since the latter couple to intramolecular vibrations of BEDT-TTF, the analysis of both electronic and vibrational features provides a tool to disentangle these contributions and to follow their temperature and electronic-correlation dependence. Calculations based on the cluster model support our interpretation.

DOI: 10.1103/PhysRevB.76.165113

PACS number(s): 74.70.Kn, 71.30.+h, 74.25.Gz, 71.10.Hf

## I. INTRODUCTION

The physics of strongly correlated electron systems is a very active field in solid-state science where the vicinity of Mott-insulating, magnetically ordered, and superconducting ground states is most intriguing. These effects are intensively studied for transition-metal oxides, particularly high-temperature superconductors and organic conductors. It is extremely interesting that all of these materials show a similar competition between ordered antiferromagnetic and superconducting phases: This suggests common physics, while the chemistry of the compounds and the origin of the conducting electrons are different.<sup>1-3</sup> These facts have initiated our investigation of the molecular conductors of the BEDT-TTF family as model compounds to study the physics of correlated electrons close to the Mott transition in two dimensions.<sup>4,5</sup>

In the  $\kappa$ -phase crystals, conducting layers of cationic bis-(ethylenedithio)tetrathiafulvalene (BEDT-TTF) molecules are separated by “charge-reservoir” layers of monovalent anions. As depicted in Fig. 1, two BEDT-TTF<sup>0.5</sup> molecules form confacial dimers which can be considered as lattice sites; due to this dimerization, the quarter-filled band originating from the overlap of the molecular orbitals of the neighboring molecules splits into a lower one, which is completely filled, and an upper conduction band, which is half filled. The anions size sensitively influences the physical properties of the system very similar to the variation of pressure since they define the spacing between the molecules (molecular sites) and thus the width of the band.<sup>6,7</sup> The ratio

of electronic correlations to the width of the conduction band is the control parameter<sup>3</sup> in the phase diagram depicted in Fig. 2. The ground state of  $\kappa$ -(BEDT-TTF)<sub>2</sub>X salts can be switched between an antiferromagnetic insulating, a superconducting, and a metallic state. These salts exhibit the highest superconducting transition temperature of all organic superconductors with  $T_c=12.5\text{ K}$ .<sup>1,2</sup>

At ambient temperature, the studied  $\kappa$ -phase BEDT-TTF salts have common properties, which may be characterized

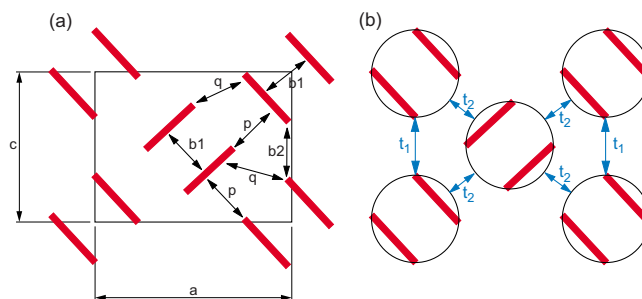


FIG. 1. (Color online) (a) Structural arrangement of the BEDT-TTF molecules in the  $\kappa$  phase (looking along the molecular axis); the size of the unit cell is approximately  $12.9\text{ \AA}$  in the  $a$  direction,  $8.5\text{ \AA}$  along the  $c$  axis, and  $30.0\text{ \AA}$  in the third direction. The overlap integrals are labeled according to Mori *et al.* (Ref. 6). The interdimer overlap integral  $b_1$  is around  $0.027$ , along the dimer chains  $b_2 \approx 0.010$ , while  $p$  and  $q$  link orthogonal molecules with approximately  $0.011$  and  $0.004$ , respectively. (b) Triangular lattice for the dimer model of  $\kappa$ -(BEDT-TTF)<sub>2</sub>X. There is hopping along the stacks  $t_1$  and along the diagonals  $t_2$ .

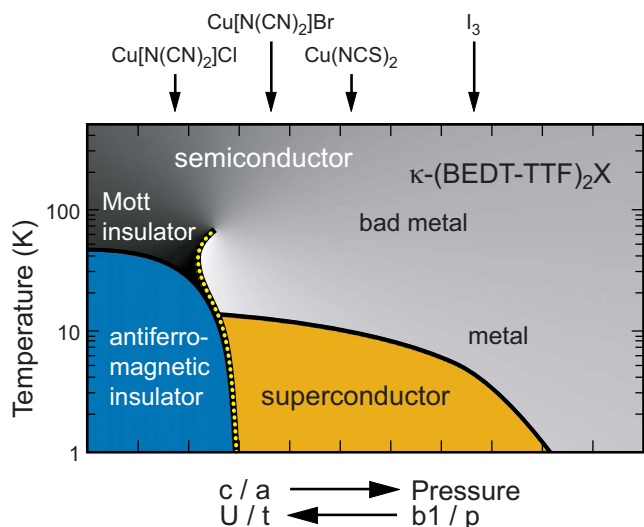


FIG. 2. (Color online) Schematic phase diagram of the  $\kappa$ -phase salts  $(\text{BEDT-TTF})_2\text{X}$ . Instead of tuning the external pressure, the same ambient-pressure ground state can be achieved by modifying the anions X. The arrows indicate the approximate position of  $\kappa\text{-(BEDT-TTF)}_2\text{Cu}[\text{N}(\text{CN})_2]\text{Cl}$ ,  $\kappa\text{-(BEDT-TTF)}_2\text{Cu}[\text{N}(\text{CN})_2]\text{Br}$ ,  $\kappa\text{-(BEDT-TTF)}_2\text{Cu}(\text{NCS})_2$ , and  $\kappa\text{-(BEDT-TTF)}_2\text{I}_3$  at ambient pressure, respectively. At room temperature, all of the compounds are moderately good conductors ( $\rho_{\text{dc}} \approx 1 \Omega \text{ cm}$ ). While  $\kappa\text{-(BEDT-TTF)}_2\text{Cu}[\text{N}(\text{CN})_2]\text{Cl}$  becomes increasingly insulating and exhibits a weak magnetic order below 35 K,  $\kappa\text{-(BEDT-TTF)}_2\text{Cu}[\text{N}(\text{CN})_2]\text{Br}$  crosses over to a metallic behavior below 100 K and eventually enters a superconducting state at  $T_c = 12 \text{ K}$ . The phase transition between the (antiferromagnetic) Mott insulator and the metal/superconductor can be explored by gradually replacing Cl by Br in  $\kappa\text{-(BEDT-TTF)}_2\text{Cu}[\text{N}(\text{CN})_2]\text{Br}_x\text{Cl}_{1-x}$ . Here,  $c$  and  $a$  are the lattice parameters;  $b1$  and  $p$  indicate the transfer integral according to Fig. 1(a).  $U/t$  is the on-site Coulomb repulsion with respect to the hopping integral  $t$ .

as a narrow-gap semiconductor or a “bad metal.” When the temperature drops below a so-called coherence temperature  $T_{\text{coh}} \approx 50 \text{ K}$  on the right side of the phase diagram, the metallic behavior becomes dominant due to the formation of Fermi liquid quasiparticles<sup>8,9</sup> until a second-order transition occurs to a superconducting state. The nature of superconductivity in organic crystals has been subject to discussion for 20 years,<sup>10</sup> but in the present study we focus on the metallic and insulating states. On the left side of the phase diagram (Fig. 2), i.e., for larger values of  $U/t$ , the system never shows metallic properties but is gradually driven into an insulating state by electronic correlations as the temperature drops below 90 K; at  $T_N \approx 35 \text{ K}$ , magnetic order is observed. A final exploration of the antiferromagnetic ground state of  $\kappa\text{-(BEDT-TTF)}_2\text{Cu}[\text{N}(\text{CN})_2]\text{Cl}$  is still lacking. NMR measurements in deuterated samples  $\kappa\text{-(}d_8\text{-BEDT-TTF)}_2\text{Cu}[\text{N}(\text{CN})_2]\text{Br}$  (which fall right on the phase boundary) revealed that at low temperatures the transition between the commensurate antiferromagnet and pseudogapped superconductor is of first order.<sup>11</sup> For  $\kappa\text{-(BEDT-TTF)}_2\text{Cu}[\text{N}(\text{CN})_2]\text{Cl}$ , electronic correlations are even stronger; nevertheless, hydrostatic pressure of only 300 bar is suf-

ficient to drive the system to the metallic and superconducting states. Most recently, enormous research efforts were dedicated to the metal-to-insulator transition and critical end point in this highly correlated two-dimensional electron system. The critical behavior in the vicinity of the Mott transition was investigated by dc measurements under external pressure and in magnetic field.<sup>12–14</sup> The alloyed series  $\kappa\text{-(BEDT-TTF)}_2\text{Cu}[\text{N}(\text{CN})_2]\text{Br}_x\text{Cl}_{1-x}$  studied in the present work, covers the most interesting region of the phase diagram spanned by the pure Cl and Br salts, including the border between the Mott insulating and metallic phases. Our infrared reflection measurements of a series of compounds with Br concentration  $x$  varying between 0% and 90% make it possible to explore the temperature and correlation (bandwidth)-dependent charge dynamics on crossing this phase boundary, as well as the unusual physical properties in the metallic region above the superconducting transition.

Several optical experiments were performed on the pristine compounds  $\kappa\text{-(BEDT-TTF)}_2\text{Cu}[\text{N}(\text{CN})_2]\text{Br}$  and  $\kappa\text{-(BEDT-TTF)}_2\text{Cu}[\text{N}(\text{CN})_2]\text{Cl}$  over the years.<sup>15–21</sup> They gave a general idea of the electronic excitation observed in the infrared region: a broad midinfrared band around  $2500\text{--}3500 \text{ cm}^{-1}$  and a narrow Drude-like peak in the spectra of superconducting Br compound<sup>22</sup> at temperatures below 50 K. In the discussion in Sec. IV A, we review the different interpretations of the midinfrared spectra. Our investigation of the alloys gives an unambiguous assignment of the spectral features in this region, important for the analysis of the charge dynamics in these salts.  $(\text{BEDT-TTF})_2\text{Cu}[\text{N}(\text{CN})_2]\text{Br}_{0.5}\text{Cl}_{0.5}$  is the only mixed compound which has previously been investigated by infrared spectroscopy,<sup>19,23–26</sup> but only in the midinfrared range.

Here, we present a systematic optical study of the series  $\kappa\text{-(BEDT-TTF)}_2\text{Cu}[\text{N}(\text{CN})_2]\text{Br}_x\text{Cl}_{1-x}$ , with  $x$  crossing all relevant regions of the phase diagram from the insulating/antiferromagnetic to the metallic/superconducting state. Our experiments cover a broad spectral range from 50 to  $10\,000 \text{ cm}^{-1}$  and temperatures from room temperature down to  $T = 5 \text{ K}$ . This enables us to follow the response of the free and localized carriers for the different points of this phase diagram, depending on temperature and correlation-to-bandwidth ratio. While we focus on the signature of localized charge excitations here, a succeeding paper<sup>27</sup> (which we refer to as Paper II in the following) will be devoted to the dynamics of free charge carriers and the formation of the coherent quasiparticle response.

## II. EXPERIMENTS

Single crystals of the  $\kappa\text{-(BEDT-TTF)}_2\text{Cu}[\text{N}(\text{CN})_2]\text{Br}_x\text{Cl}_{1-x}$  salts were grown by standard electrochemical methods. Certain ratios of Br/Cl concentration were chosen to obtain a series of alloys. Subsequent to the optical reflection experiments, each individual crystal was checked by microprobe analysis in order to determine the composition. The actual Br/Cl ratio turned out to be significantly different than expected from the starting concentration since Br enters the compounds much easier than Cl.<sup>28</sup> It was hardly possible to produce samples with pre-

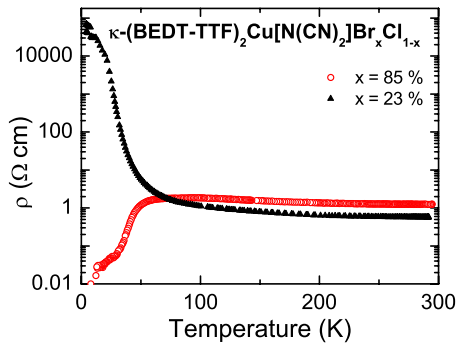


FIG. 3. (Color online) dc resistivity versus temperature of  $\kappa$ -(BEDT-TTF) $_2$ Cu[N(CN) $_2$ ]Br $_x$ Cl $_{1-x}$  and  $\kappa$ -(BEDT-TTF) $_2$ Cu[N(CN) $_2$ ]Br $_{0.85}$ Cl $_{0.15}$ . While the latter compound becomes metallic below 100 K and eventually superconducting at  $T_c \approx 12$  K, the former one gradually turns insulating.

defined Br concentration. In the following, we denote the actual Br content of  $\kappa$ -(BEDT-TTF) $_2$ Cu[N(CN) $_2$ ]Br $_x$ Cl $_{1-x}$ , where  $x=0\%$ , 40%, 73%, 85%, and 90%; the concentration was found homogeneous for each specimen. The platelets contained naturally flat ( $ac$ ) surfaces with a typical size of about  $1 \times 1$  mm $^2$ .<sup>29</sup> The orientation was determined from the optical spectra.

The strong dependence of the dc resistivity on the Br/Cl ratio is emphasized in Fig. 3, where  $\rho(T)$  is plotted for a crystal with low ( $x=23\%$ ) and high ( $x=85\%$ ) bromine content. For the insulating sample  $\kappa$ -(BEDT-TTF) $_2$ Cu[N(CN) $_2$ ]Br $_{0.23}$ Cl $_{0.77}$ , the resistivity rises by many orders of magnitude as the temperature decreases, most dramatically below 70 K. On the contrary,  $\kappa$ -(BEDT-TTF) $_2$ Cu[N(CN) $_2$ ]Br $_{0.85}$ Cl $_{0.15}$  shows basically the same temperature dependence like the pure Br specimen:  $\rho(T)$  increases slightly below room temperature until it reaches a broad maximum around 100 K. At lower temperatures, the behavior is metallic with  $\rho(T) \propto T^2$  for  $T < 35$  K, and finally a superconducting transition is observed at  $T_c \approx 12$  K.<sup>30</sup> The superconducting properties of  $\kappa$ -(BEDT-TTF) $_2$ Cu[N(CN) $_2$ ]Br $_x$ Cl $_{1-x}$  with different Br concentrations have been investigated previously by dc resistivity and magnetization.<sup>34</sup>

The in-plane optical reflectivity was measured with light polarized along  $a$  and  $c$  axes. Employing a modified Bruker IFS 113v Fourier-transform spectrometer, we covered a broad frequency range from 50 to 10 000 cm $^{-1}$  (6 meV–1.2 eV) with a resolution of up to 0.5 cm $^{-1}$ . The single crystals were studied at 300, 150, 90, 50, 35, 20, and 5 K with the help of a cold-finger cryostat. To achieve good thermal contact, the samples were fixed by carbon paste on a brass cone directly attached to the cold finger. Absolute values of the reflectivity are obtained by subsequently evaporating gold onto the sample and remeasuring it as a reference mirror at all temperatures.<sup>35</sup> The *in situ* gold-evaporation technique is more accurate than other referencing methods because it utilizes the entire sample surface and is less affected by surface imperfections. In addition, for the crystals with 40% and 85% Br concentration, reflectivity spectra were measured in

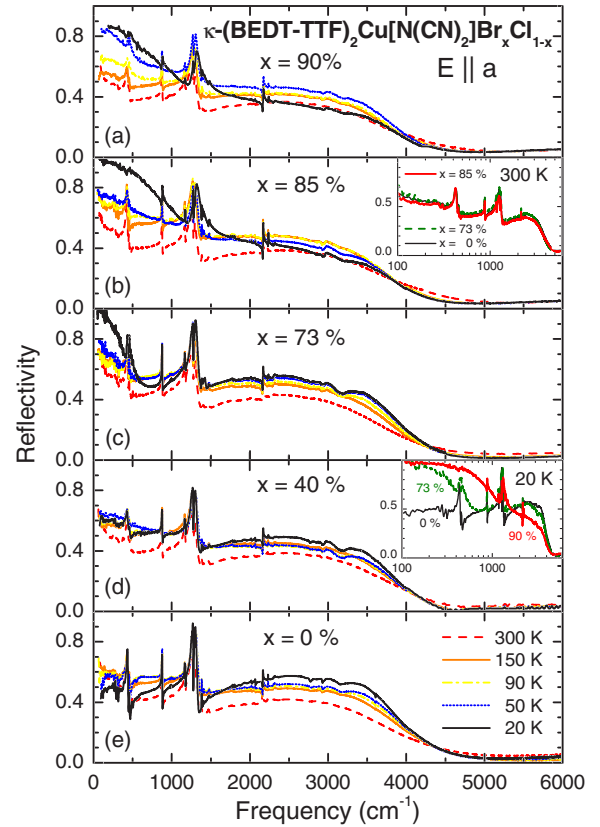


FIG. 4. (Color online) Reflectivity spectra of  $\kappa$ -(BEDT-TTF) $_2$ Cu[N(CN) $_2$ ]Br $_x$ Cl $_{1-x}$  for the polarization  $E \parallel a$  measured at various temperatures:  $T=300, 150, 90, 50,$  and  $20$  K. Panels (a)–(e) correspond to different Br concentrations:  $x=90\%, 85\%, 73\%, 40\%,$  and  $0\%$ . The insets show the room-temperature and low-temperature spectra for  $x=90\%, 73\%,$  and  $0\%$  on a logarithmic frequency scale.

2000–12 000 cm $^{-1}$  range at temperatures between 300 and 20 K using a Bruker IFS 66v spectrometer equipped with an IR microscope and cold-finger Cryovac Microstat. The spectra in this range coincide for both methods of measurement; there is basically no dependence on Br content and temperature. In the overlapping range, they are in agreement with the room-temperature data received by Drozdova *et al.*<sup>24</sup> up to 40 000 cm $^{-1}$ . These spectra were also used as a high-frequency extrapolation for the other compounds. From the reflectivity spectra, the optical conductivity was calculated employing a Kramers-Kronig analysis.<sup>36</sup> At low frequencies, the data were extrapolated by the Hagen-Rubens behavior, which was double checked by the dc resistivity obtained from standard four-probe measurements (Fig. 3). The low-frequency extrapolation only very weakly affects the spectra in the measured range, i.e., the absolute values of conductivity.

### III. RESULTS

In Figs. 4 and 5, the reflectivity and conductivity spectra of  $\kappa$ -(BEDT-TTF) $_2$ Cu[N(CN) $_2$ ]Br $_x$ Cl $_{1-x}$  (with  $x=0\%, 40\%, 73\%, 85\%,$  and  $90\%$ ) are plotted for light polarized parallel

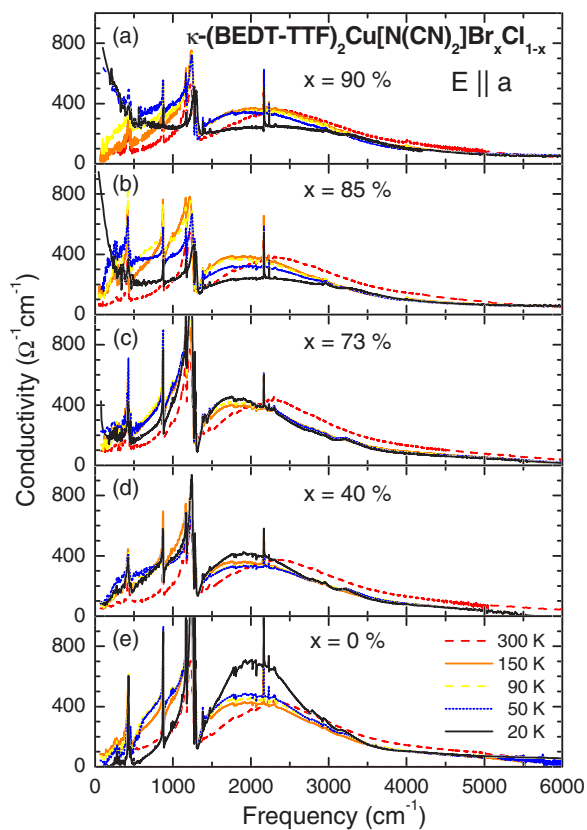


FIG. 5. (Color online) Optical conductivity spectra ( $E||a$ ) of  $\kappa$ -(BEDT-TTF) $_2$ Cu[N(CN) $_2$ ]-Br $_x$ Cl $_{1-x}$  at different Br concentrations  $x$  and temperatures, obtained by a Kramers-Kronig analysis from the data of Fig. 4.

to the  $a$  direction at distinct temperatures from 300 down to 20 K. Because there is no significant difference between the  $T=20$  and 5 K spectra, we omitted the latter. At ambient temperature, the optical properties only weakly depend on the Br content [inset of Fig. 4(b)]. As expected for semiconductors, the reflectivity is basically frequency independent at small frequencies, and hence the corresponding room-temperature conductivity is low; the reflectivity starts to decrease significantly above 3500  $\text{cm}^{-1}$  and reaches a value close to zero in both polarizations around 5000  $\text{cm}^{-1}$ . The respective conductivity spectra show a broad absorption band centered between 2000 and 3000  $\text{cm}^{-1}$ , which is well documented in literature for the  $\kappa$ -phase of BEDT-TTF salts in general. The strong absorption features observed in the midinfrared around 400, 850, and 1400  $\text{cm}^{-1}$  are totally symmetric vibrations of the BEDT-TTF molecule, activated by electron-molecular vibrational (emv) coupling (Ref. 5, and references therein); we will give a detailed analysis in Sec. IV C.

Significant changes of the optical spectra are observed when cooling the samples below  $T=90$  K. The far-infrared reflectivity strongly increases for specimens with high Br content (Fig. 4), while the midinfrared reflectivity is suppressed. Correspondingly, as seen in Fig. 5, a Drude-like contribution develops in the conductivity spectra of the samples with  $x=73\%$ , 85%, and 90% at low temperatures. The latter compound exhibits a behavior similar to the pris-

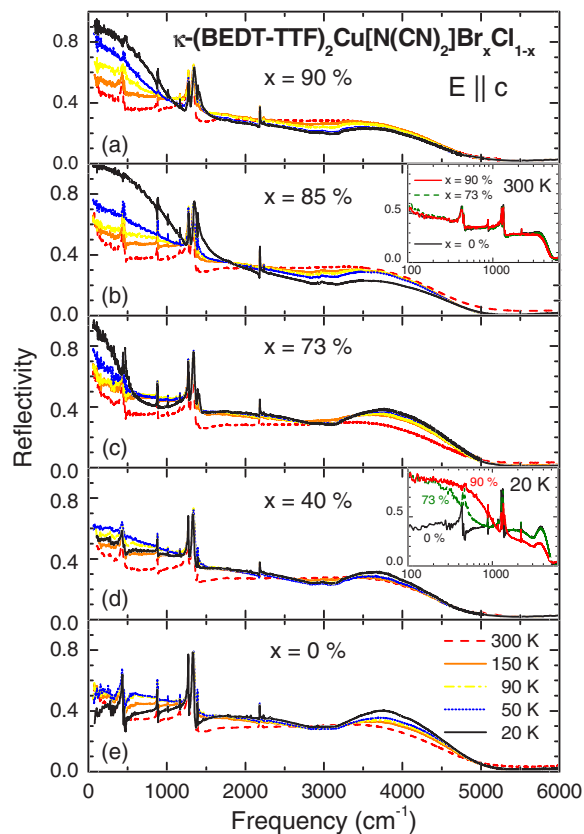


FIG. 6. (Color online) Reflectivity spectra of  $\kappa$ -(BEDT-TTF) $_2$ Cu[N(CN) $_2$ ]-Br $_x$ Cl $_{1-x}$  for light polarized  $E||c$  measured at various temperatures as indicated. The different panels (a)–(e) correspond to Br concentrations:  $x=90\%$ , 85%, 73%, 40%, and 0%. The insets show the room-temperature and low-temperature spectra on a logarithmic frequency scale.

tine  $\kappa$ -(BEDT-TTF) $_2$ Cu[N(CN) $_2$ ]-Br salt.<sup>15</sup> The opposite is observed for the salts with low Br content: The far-infrared reflectivity drops while it rises in midinfrared. The absolute values of reflectivity and conductivity are slightly enhanced compared to previously published results.<sup>15,17–21</sup> This we attribute to our advanced *in situ* gold-evaporation method for the reference measurement which also accounts for imperfections of the crystal surface.

The reflectivity and conductivity for the perpendicular polarization ( $E||c$ ) are shown in Figs. 6 and 7 for different Br concentrations  $x$  and temperatures  $T$ . The spectra exhibit basically the same features as the ones recorded along the  $a$  direction, except that the shape of the midinfrared absorption is different. As previously reported, for most other  $\kappa$  salts, the maximum of the absorption band for the  $c$  axis lies at higher frequencies. While at ambient temperature a distinction is difficult, at low temperatures it becomes obvious from both reflectivity and conductivity data that it consists of two components: In addition to the band around 2000  $\text{cm}^{-1}$ , a second narrower mode has its maximum around 3500  $\text{cm}^{-1}$ . This behavior is most pronounced for the pure Cl compound. Again, with increasing Br content, a Drude contribution develops as the temperature is reduced below 50 K.

We want to point out that the accessible frequency range of our experiments is limited to  $\nu \geq 50$   $\text{cm}^{-1}$  due to the small

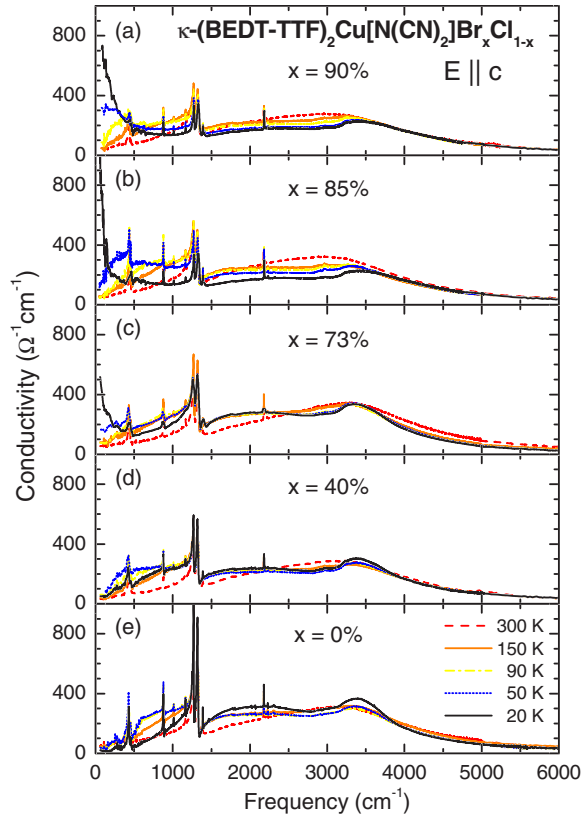


FIG. 7. (Color online) Optical conductivity spectra ( $E \parallel c$ ) for  $\kappa\text{-(BEDT-TTF)}_2\text{Cu}[\text{N}(\text{CN})_2]\text{Br}_x\text{Cl}_{1-x}$  of different Br concentrations: (a)  $x=90\%$ , (b)  $85\%$ , (c)  $73\%$ , (d)  $40\%$ , and (e)  $0\%$  measured at various temperatures:  $T=300$ ,  $150$ ,  $90$ ,  $50$ , and  $20$  K. The midinfrared band clearly has two contributions.

sample surfaces. Thus, we cannot detect the superconducting energy gap  $\Delta_0$ , which is expected around  $2\Delta_0=3.53k_B T_c \approx 30\text{ cm}^{-1}$ .

#### IV. DISCUSSION

Despite the above mentioned limitations, our data cover a very broad frequency range from  $50$  to  $10\,000\text{ cm}^{-1}$ . Therefore, we are able not only to study the vibrational features and the midinfrared absorption, but also to analyze the temperature and doping dependence of the Drude contribution in  $\kappa\text{-(BEDT-TTF)}_2\text{Cu}[\text{N}(\text{CN})_2]\text{Br}_x\text{Cl}_{1-x}$ . However, since there is no agreement in the literature on the interpretation of the midinfrared absorption band, which is important for an analysis of the whole charge dynamics in these materials, we first address this part of the spectra. The contribution of the itinerant electrons will be analyzed extensively and discussed in Paper II.

The common approach is to fit the optical spectra by the Drude-Lorentz model<sup>5,36</sup> because it helps to disentangle the contributions of conduction electrons, interband transitions and vibrational features. As an example, the optical conductivity along the  $c$  direction of the crystal with  $x=0.85$  is displayed in Fig. 8 together with a fit by one Drude-like component and several Lorentzian oscillators; to further re-

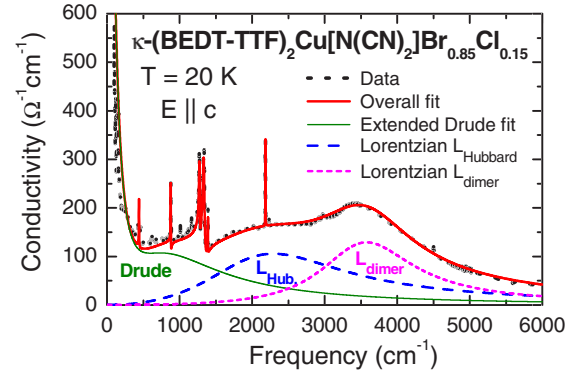


FIG. 8. (Color online) Fit of the frequency dependent conductivity of  $\kappa\text{-(BEDT-TTF)}_2\text{Cu}[\text{N}(\text{CN})_2]\text{Br}_{0.85}\text{Cl}_{0.15}$  at  $20\text{ K}$  for the electric field polarized parallel to the  $c$  axis.  $L_{\text{dimer}}$  and  $L_{\text{Hubbard}}$  show the two Lorentz oscillators required to fit the midinfrared peak. The narrow lines describe the vibrational features. In addition, an extended Drude model is included for the low-frequency increase.

strict the parameters, the  $R(\omega)$  and  $\sigma(\omega)$  spectra were fitted simultaneously. This procedure was applied to the spectra taken in both polarization directions and at all temperatures and values of Br doping.

#### A. Midinfrared band: Overview of the different interpretations

In general, the most prominent feature in the optical conductivity spectra of  $\kappa$ -phase BEDT-TTF salts is the broad midinfrared hump. It peaks around  $2200\text{ cm}^{-1}$  for the polarization  $E \parallel a$  and at  $3200\text{ cm}^{-1}$  in the  $c$  direction, where it exhibits a more complicated double structure. Albeit it seems obvious—in particular, when cooling down—that two contributions add up for this band, the explanations proposed over the years took into account only one single process. It was suggested that the midinfrared peak is due to charge transfer inside the dimer<sup>15–17,37,38</sup> or due to transitions between the Hubbard bands formed by the correlated conduction electrons.<sup>21,39,40</sup>

Eldridge and co-workers<sup>15,17</sup> first suggested that the midinfrared peak is due to charge-transfer bands, with the excitations confined to the dimers and the charge transfer occurring between adjacent molecules. The polarization dependence is explained by different interactions between neighboring dimers [Fig. 1(a)]. The arguments were supported by electronic band-structure calculations of the  $\kappa$ -phase salts performed by Whangbo and co-workers on the basis of the tight-binding approximation.<sup>41,42</sup> The highest occupied band is half filled with only very little difference in bandwidth and density of states at the Fermi level when going from  $\kappa\text{-(BEDT-TTF)}_2\text{Cu}[\text{N}(\text{CN})_2]\text{Cl}$  to  $\kappa\text{-(BEDT-TTF)}_2\text{Cu}[\text{N}(\text{CN})_2]\text{Br}$ . Obviously, this is a very rough approximation which can explain neither the semiconducting behavior at ambient temperature nor a redistribution of the spectral weight from this midinfrared maximum to the Drude peak for compounds with high Br concentration on cooling (discussed in Paper II) nor the different ground states of the compounds.

A more consistent picture was achieved when both components of the optical conductivity, the Drude-like contribution, and the midinfrared hump were explained in the framework of a half-filled two-dimensional system with strong electronic correlations.<sup>4,6,43</sup> The structure of the  $\kappa$  phase was mapped on an anisotropic triangular lattice, each site presenting one dimer, as depicted in Fig. 1(b). The interdimer overlap integrals define the hopping  $t$  between the sites of a triangular half-filled lattice considered by theory, they are  $t_1 = 30$  meV and  $t_2 = 50$  meV.<sup>4,43</sup> The intradimer overlap plays the role of the effective on-site Coulomb interaction  $U_{\text{eff}}$ .<sup>6,43,44</sup> Consequently,  $U_{\text{eff}}$  increases with dimerization: for the Cl analog,  $b_1$  is slightly higher which causes larger  $U_{\text{eff}}$ . *Ab initio* calculations by Fortunelli and Painelli<sup>45</sup> give the value of  $U_{\text{eff}} = 0.4$  eV for a dimer in  $\kappa$ -(BEDT-TTF)<sub>2</sub>Cu[N(CN)<sub>2</sub>]Br; this is in agreement with experiments.

It has been predicted by theory that the Mott-insulator transition in a two-dimensional lattice typically occurs when  $U$  is comparable to the bandwidth  $W = 8t$ . In the present case,  $U_{\text{eff}}/t \approx 8$ , implying that we are very close to the metal-insulator transition.  $U_{\text{eff}}/t$  increases when going from Br to Cl anions, i.e., moving from right to left in the phase diagram (Fig. 2), and leads to the localization of the charge carriers.<sup>46</sup> Following these considerations, recently,<sup>21</sup> the experimentally observed midinfrared band around 3000 cm<sup>-1</sup> was associated with the transition between the Hubbard bands at  $\hbar\omega \approx U_{\text{eff}}$ .

The application of the dynamical mean-field theory to the metallic side of the phase diagram suggests<sup>9,40</sup> that besides the midinfrared band around  $U_{\text{eff}}$ , a quasiparticle peak at the Fermi level grows with temperature below  $T_{\text{coh}} \approx 0.1t^*$ , where  $t^*$  is the overlap integral. Due to transitions between the coherent quasiparticle band and the Hubbard bands, a new peak is supposed to develop around  $\hbar\omega \approx U_{\text{eff}}/2$  for  $T < T_{\text{coh}}$ .

### B. Midinfrared band: Our experimental results

Our present investigation of the substitution series  $\kappa$ -(BEDT-TTF)<sub>2</sub>Cu[N(CN)<sub>2</sub>]Br<sub>*x*</sub>Cl<sub>1-*x*</sub> sheds light on the above formulated controversy because all features were traced when going from the metallic to the insulating phase both by changing temperature  $T$  and the relative correlation strength  $U/t$ . This enabled us to disentangle the components coming from charge transfer inside the (BEDT-TTF)<sub>2</sub> dimers and between the dimers. We propose that the observed optical response is explained by two contributions: (i) One is the carriers which belong to the upper conductance half-filled band. These are the carriers which move between the dimers (lattice sites) and define the two-dimensional metallic properties. However, in the Mott-insulating state, the strong electronic repulsion immobilizes and eventually confines them. (ii) The other is the carriers which are localized on the dimers (lattice sites) [Fig. 1(b)]. We propose that the intradimer transitions cause the high-frequency contribution  $L_{\text{dimer}}$ , while the band  $L_{\text{Hubbard}}$  at lower frequencies is ascribed to interdimer transitions, i.e., to the transitions between the Hubbard bands.

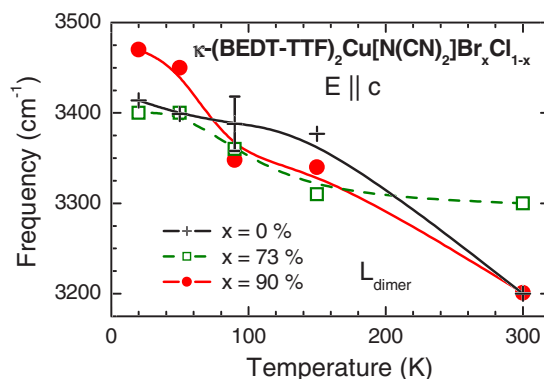


FIG. 9. (Color online) Temperature dependence of the midinfrared peak  $L_{\text{dimer}}$  in  $\kappa$ -(BEDT-TTF)<sub>2</sub>Cu[N(CN)<sub>2</sub>]Br<sub>*x*</sub>Cl<sub>1-*x*</sub>, with  $x = 0\%$ , 73%, and 90% obtained by a Lorentzian fit for the polarization  $E \parallel c$ . The lines are guides to the eye.

Generally, the band of the intradimer transition is expected to appear at higher frequencies compared to the transition between the dimers. It was already shown for molecular chains that the high-frequency band vanishes when the dimerization is reduced;<sup>47</sup> calculations were also performed on a two-dimensional  $\kappa$ -like structure, leading to similar conclusions.<sup>48</sup> The same result is obtained by the cluster model,<sup>49</sup> when extending it to tetramers and hexamers; the electronic transitions summing up the intradimer and interdimer excitations shift to lower frequencies and get broader compared to the pure intradimer one.

In both reflectivity and conductivity spectra (Figs. 6–8) for light polarized parallel to the  $c$  axis, two bands can be clearly distinguished: a narrow high-frequency peak  $L_{\text{dimer}}$  and a broad peak  $L_{\text{Hubbard}}$  located at lower frequencies. Contrary, in  $a$  direction, there is no clear separation visible between  $L_{\text{dimer}}$  and  $L_{\text{Hubbard}}$  in the optical spectra (Figs. 4 and 5). Such an anisotropy in the midinfrared range is well documented for these  $\kappa$  salts.<sup>5,50</sup> However, the detailed analysis based on the cluster model given below will show that despite the anisotropy, both peaks are present in either orientations.

The temperature dependence of the  $L_{\text{dimer}}$  frequency ( $E \parallel c$ ) is plotted in Fig. 9 for different Br concentrations. Within the uncertainty of the Lorentz fit, at ambient temperature the position of the high-frequency oscillator  $L_{\text{dimer}}$  does not show a distinct dependence on the Br content along the  $c$  axis; also, the oscillator strength of this band does not vary substantially. In general, there is an upward shift of approximately 100 to 200 cm<sup>-1</sup> when going down to  $T = 20$  K. We attribute this blueshift to the thermal contraction of the single crystals, which slightly enhances the intradimer transfer integral  $b_1$  [Fig. 1(a)]; i.e., the intradimer overlap increases.<sup>6</sup> The difference between metallic and insulating compounds is seen at 50 K and lower: While the temperature dependent high-frequency shift of  $L_{\text{dimer}}$  is more enhanced upon cooling in the metallic samples with  $x = 90\%$  and 85%, it levels off for the insulating ones with low Br concentration. Obviously, the  $L_{\text{dimer}}$  oscillator frequency is not considerably affected by the opening of the Mott-Hubbard gap at  $T \leq 50$  K, which results in an increase of the dc resistivity of several orders of magnitude.

The intradimer transition, i.e., a charge transfer between the two face-to-face arranged BEDT-TTF molecules, is expected to be strongly coupled to the totally symmetric molecular vibrations. Thus, a detailed analysis of the experimentally obtained temperature dependence of their spectra and a comparison to the theoretical predictions of the cluster model will be the key to a final assignment of the electronic features in the spectra.

### C. Vibrational features

The sharp absorption features in the frequency range between 400 and 1600  $\text{cm}^{-1}$  are known to be totally symmetric vibrations activated by coupling with electronic excitations. In the course of numerous vibrational studies on the  $\kappa$ -phase BEDT-TTF salts, Eldridge and co-workers<sup>18,37,51,52</sup> and others<sup>20,24</sup> presented a complete assignment of the totally symmetric vibrations. Here, we use the  $C_{2h}$  symmetry assignment which takes a deformation of a BEDT-TTF molecule inside the crystal into account.<sup>53</sup> In our work, we could follow not only the temperature but also the doping dependence of these features, which improves our interpretation of the spectra.

The most prominent  $\nu_4(A_g)$  vibration involves a symmetric stretching of the C=C double bonds; in the spectra in Fig. 10, it appears as a double peak due to the  $\nu_6$  antiresonance. We estimate the center frequency of the  $\nu_4(A_g)$  band by fitting the complete feature with a Lorentzian, disregarding the antiresonances for a moment.<sup>59</sup> The accuracy of this procedure is limited to  $\pm 1 \text{ cm}^{-1}$  and strongly depends on temperature, compound, and polarization; nevertheless, it allows us to extract the general tendency. At room temperatures, the  $\nu_4(A_g)$  mode is observed at about 1240  $\text{cm}^{-1}$  along the  $a$  axis and at 1280  $\text{cm}^{-1}$  along the  $c$  axis in the spectra of the  $\kappa$ -(BEDT-TTF)<sub>2</sub>Cu[N(CN)<sub>2</sub>]Br<sub>*x*</sub>Cl<sub>1-*x*</sub>. As can be seen from Figs. 11(a) and 11(c), with decreasing temperature (300 K  $\leq T < 50$  K), the  $\nu_4(A_g)$  modes slightly shift to higher frequencies in about the same manner for all compounds. As  $T$  is reduced, this tendency enhances further for  $x=85\%$  and 90%: The total shift amounts to approximately 45  $\text{cm}^{-1}$  for  $E \parallel a$  and less than 5  $\text{cm}^{-1}$  in the  $c$  direction; the variation saturates at very low temperatures. For the insulating compounds with low Br content, the  $\nu_4(A_g)$  mode even reverses its temperature dependence below  $T_{\text{coh}} \approx 50$  K and becomes softer. Except for some gradual difference, the behavior is very similar for both orientations. Below 50 K, the  $\nu_4(A_g)$  mode becomes sharper in the insulating samples, while it broadens and seems to be weaker for high Br content.

The frequency of the  $\nu_6(A_g)$  mode (vibration of the CH<sub>2</sub> groups) overlaps with the broad emv-coupled  $\nu_4(A_g)$  band. In Fig. 10, the excitation is seen as an antiresonance around 1270 to 1280  $\text{cm}^{-1}$  for  $E \parallel a$  and slightly higher for the perpendicular direction. At low temperatures, four bands of  $\nu_6(A_g)$  are resolved, originating from four distinct CH<sub>2</sub> groups per unit cell. We follow the temperature dependence by choosing the minimum around 1273  $\text{cm}^{-1}$ . Again, for low Br content the  $\nu_6(A_g)$  mode gradually moves down in frequency with decreasing temperature, while it significantly shifts to higher values for  $x=85\%$  and 90%, as presented in

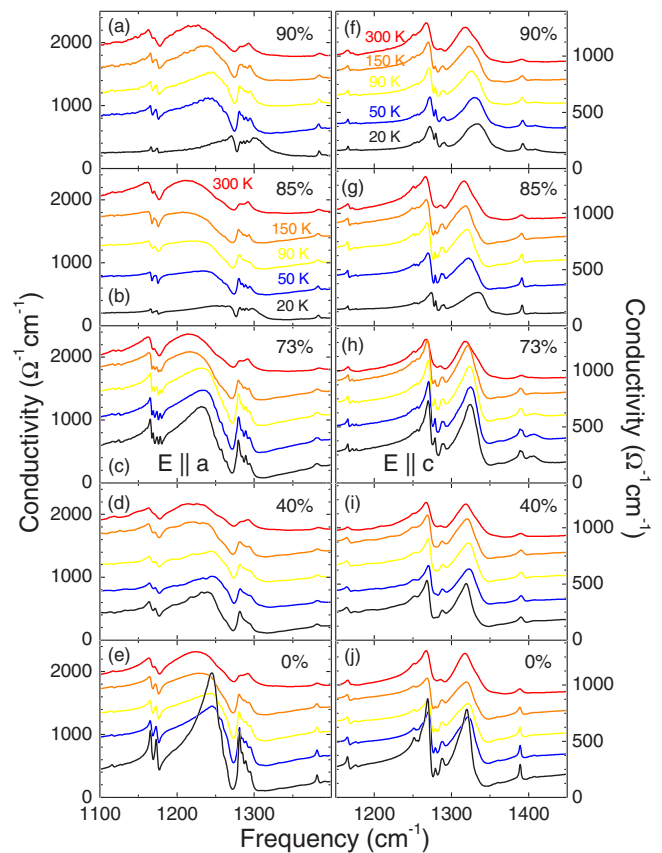


FIG. 10. (Color online) Detailed view of the optical conductivity of  $\kappa$ -(BEDT-TTF)<sub>2</sub>Cu[N(CN)<sub>2</sub>]Br<sub>*x*</sub>Cl<sub>1-*x*</sub> along the  $a$  and  $c$  directions (left and right panels, respectively) for different Br concentrations  $x=90\%$ , 85%, 73%, 40%, and 0%, (a)–(e) and (f)–(j), respectively. The spectra for the different temperatures (bottom to top:  $T=20, 50, 90, 150,$  and 300 K) are offset by 400 ( $\Omega \text{ cm}^{-1}$ ) for clarity.

Fig. 11(c). The same temperature dependence of  $\nu_6(A_g)$  is observed parallel to  $c$  [Fig. 11(d)]. A similar temperature and Br-concentration dependence is seen for the peaks of the emv-coupled “ring-breathing” mode  $\nu_{10}(A_g)$  of the BEDT-TTF molecule<sup>58</sup> at 870 and 885  $\text{cm}^{-1}$  and of the  $\nu_{13}(A_g)$  at about 430  $\text{cm}^{-1}$ . Accordingly, the peaks are pretty intense in the insulating state and are less significant in the spectra for high Br concentration.

In contrast to the emv-coupled modes, the infrared active  $\nu_{45}(B_{2u})$  vibration of the BEDT-TTF molecule detected around 1383  $\text{cm}^{-1}$  (Fig. 10) and the CN-stretch vibration of the anion layer observed around 2160  $\text{cm}^{-1}$  do not depend on the Br concentration and show no pronounced temperature dependence besides the expected hardening with cooling. Therefore, since the charge on the BEDT-TTF molecules is not redistributed in  $\kappa$ -(BEDT-TTF)<sub>2</sub>Cu-[N(CN)<sub>2</sub>]Br<sub>*x*</sub>Cl<sub>1-*x*</sub> when the samples are cooled down, the characteristic temperature dependence of the emv-coupled  $A_g$  modes has to be due to the electronic excitation to which they are coupled.

### D. Excitations localized on dimers: Charge transfer and emv-coupled features

The cluster model (see, for example, Rice,<sup>60</sup> Yartsev *et al.*,<sup>49</sup> and Delhaes and Yartsev<sup>61</sup>) describes the optical prop-

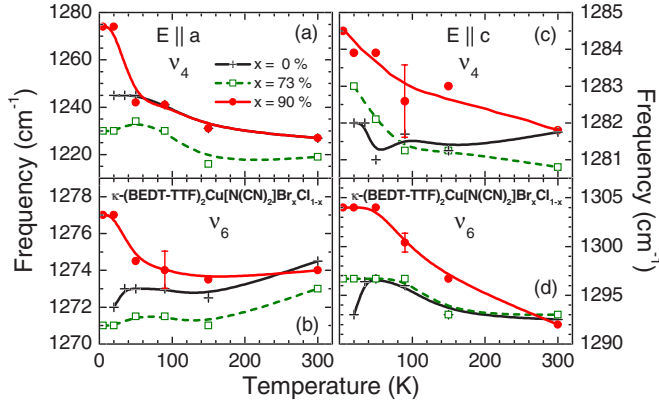


FIG. 11. (Color online) Temperature dependence of the mode frequencies of the intramolecular vibrations  $\nu_4(A_g)$  and  $\nu_6(A_g)$  for  $\kappa$ -(BEDT-TTF) $_2$ Cu[N(CN) $_2$ ]Br $_x$ Cl $_{1-x}$  with Br concentrations 0%, 73%, and 90%. (a) The  $\nu_4(A_g)$  mode along the  $a$  direction was fitted by a Lorentzian and the center frequency plotted. (b) In the case of  $\nu_6(A_g)$ , the frequencies are defined as the minima in the respective optical conductivity, i.e., the strongest of the quadruple. In frames (c) and (d), the equivalent data are presented for the polarization  $E \parallel c$ . The lines correspond to spline fits.

erties of molecular clusters with arbitrary geometry and equilibrium charge density distribution. The corresponding Hamiltonian has the following form:

$$H = H_e + H_v + \sum_{\alpha,i} g_{\alpha,i} n_i Q_{\alpha,i} - \mathbf{p} \cdot \mathbf{E}. \quad (1)$$

Here,  $H_v$  describes totally symmetric ( $A_g$ ) internal vibrations of the molecules.  $Q_{\alpha,i}$  is a dimensionless normal mode coordinate of a symmetric vibration  $\alpha$  of the  $i$  molecule with frequency  $\omega_\alpha$ . Linear emv coupling is described by the third term, where  $n_i$  is an occupation number operator for a molecule  $i$  and  $g_\alpha$  denotes coupling constants. The term  $\mathbf{p} \cdot \mathbf{E}$  gives the interaction energy of an external electric field  $\mathbf{E}$  with the induced dipole moment  $\mathbf{p}$  of a cluster.

The electronic Hamiltonian  $H_e$  is taken in the Hubbard approximation in the absence of vibronic coupling at the equilibrium values of  $Q_{\alpha,i}$ . In general, it takes into account repulsion between electrons (holes) on the same molecule  $U(U_{\text{mol}})$  and neighboring molecules  $V(V_{\text{mol}})$ , and  $t$  is a transfer integral between the molecules,

$$H_e = \sum_i \epsilon_i n_i - \sum_{i,\sigma} t_{i,i+1} (c_{i,\sigma}^\dagger c_{i+1,\sigma} + c_{i+1,\sigma}^\dagger c_{i,\sigma}) + \frac{U}{2} \sum_{i,\sigma} n_{i,\sigma} n_{i,-\sigma} + \sum_i V_{i,i+1} n_i n_{i+1}. \quad (2)$$

Using this model, the frequency dependent conductivity of the molecular clusters is calculated. It consists of two contributions: (i) a wide band due to optically activated charge transfer between the molecules in a cluster (the parameters which define this transition are the transfer integral  $t$  between the molecules and the Coulomb repulsion  $U_{\text{mol}}$  of two electrons on one molecule) and (ii) comparatively narrow features due to  $A_g$  intramolecular vibrations which become infrared active by emv coupling to the charge-transfer

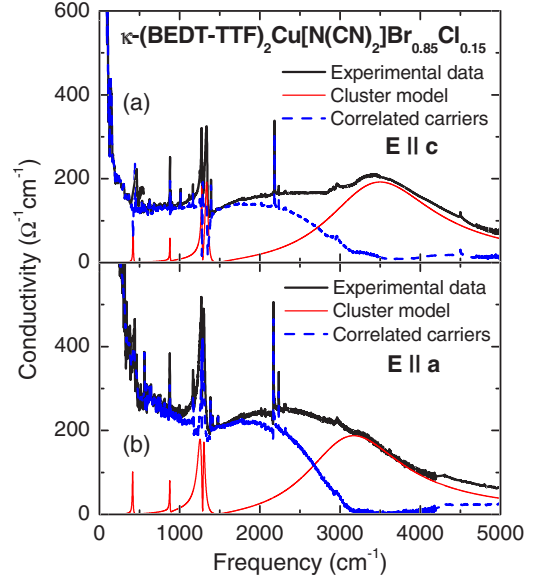


FIG. 12. (Color online) Conductivity of  $\kappa$ -(BEDT-TTF) $_2$ Cu[N(CN) $_2$ ]Br $_{0.85}$ Cl $_{0.15}$  for the two polarizations (a)  $E \parallel c$  and (b)  $E \parallel a$  at  $T = 20$  K. The solid red curves represent the conductivity for the intradimer transition and the emv-coupled modes calculated within the cluster model. The dotted blue curves show the difference between the experimental data (thick black line) and the red curve. Fit parameters for  $E \parallel c$  are  $U_{\text{mol}} = 0.5$  eV and  $t(b1) = 0.21$  eV. The vibrational frequencies  $\nu_i$  and respective coupling constants  $Q_i$  are  $\nu_4 = 1460$  cm $^{-1}$ ,  $Q_4 = 610$ ;  $\nu_6 = 1287$  cm $^{-1}$ ,  $Q_6 = 95$ ;  $\nu_{10} = 878$  cm $^{-1}$ ,  $Q_{10} = 120$ ; and  $\nu_{13} = 445$  cm $^{-1}$ ,  $Q_{13} = 240$ . For  $E \parallel a$ , we used  $U_{\text{mol}} = 0.5$  eV and  $t(b1) = 0.19$  eV; the frequencies and coupling constants are the same except  $Q_4 = 680$ .

excitation (they are shifted down in frequency with respect to the corresponding Raman modes).<sup>18,51,52</sup> The shift and the intensity of the emv-coupled features depend on the size of coupling constants  $g_\alpha$  and on the position of the respective charge-transfer band.

The model taking into account two perpendicular dimers of BEDT-TTF molecules successfully describes the midinfrared peak and emv-coupled features in the room-temperature spectra of the  $\kappa$ -phase salts,<sup>49,62</sup> while it does not account for the metallic behavior; thus, it is not able to mimic the appearance of a Drude peak in the compounds with high Br content.

In this work, we use the simplest dimer model to describe the emv-coupled features present also in the metallic phase and to verify the assignment of the midinfrared peak  $L_{\text{dimer}}$  to the intradimer charge transfer. As an example, in Fig. 12(a), we show a fit by the dimer model of the 85% Br compound spectra. For  $E \parallel c$ , the dimer model with  $U_{\text{mol}} = 0.5$  eV and transfer integral term  $t(b1) = 0.21$  eV can reasonably well predict both the position of the high-frequency electronic maximum  $L_{\text{dimer}}$  and of the emv-coupled features. The value of the transfer integral energy is somewhat lower than those received by the Hückel method:  $t(b1) = 0.26 - 0.27$  eV.<sup>4,6</sup> Taking into account the very different approaches of these methods, the agreement is quite good. We find that the intradimer transition is responsible for nearly all the intensity of the emv-coupled features. In the low-temperature metallic

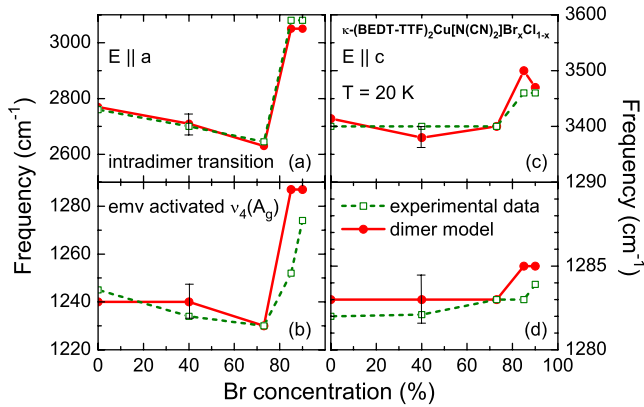


FIG. 13. (Color online) Peak position of the intradimer excitation and the emv-coupled molecular vibration  $\nu_4(A_g)$  as a function of Br concentration  $x$  as obtained from the fit of the optical spectra of  $\kappa$ -(BEDT-TTF) $_2$ Cu[N(CN) $_2$ ]Br $_x$ Cl $_{1-x}$  by the dimer model. (a) and (b) show the results for the polarization  $E||a$ , while (c) and (d) are for the  $c$  direction. In the upper frames, the frequency the intradimer absorption are displayed; in the lower frames, the mode position of the emv activated vibration  $\nu_4(A_g)$  is plotted. The experimental data are given as open squares, and the points from fit by closed dots. The lines connect the points.

state, the intradimer transition interacts strongly with the totally symmetric vibrations, while this process is less important for the charge transfer between the dimers.

In order to identify the intradimer transition band for polarization  $E||a$ , we start with the respective parameters obtained for the  $E||c$ . Only the position of the intradimer charge transfer is varied by changing the transfer integral  $b1$  until the positions of emv-coupled features, which are considerably softer along the  $a$  axis, match the experiment. Consequently, the position of the intradimer transition follows these emv-coupled vibrations. The fit with  $t(b1)=0.19$  eV suggests that the  $L_{\text{dimer}}$  has its maximum at about  $3150$   $\text{cm}^{-1}$  in the  $a$  direction, compared to  $3500$   $\text{cm}^{-1}$  found for  $E||c$ . The fit by the dimer model was performed for all compounds, temperatures, and polarization directions. Figure 13 illustrates the correlation between the position of the charge-transfer band [Figs. 13(a) and 13(c)] and the emv activated  $\nu_4(A_g)$  vibration [Figs. 13(b) and 13(d)] at low temperatures. In both polarizations, their frequencies strongly depend on the Br content in  $\kappa$ -(BEDT-TTF) $_2$ Cu[N(CN) $_2$ ]Br $_x$ Cl $_{1-x}$ . The strong shift of the peaks to higher frequencies for the metallic compounds is clearly seen. The figure also demonstrates the very good agreement between experiment and calculations.

For a further analysis of the data focusing on itinerant charge carriers, we subtract the results of the cluster-model calculations from the experimental data. As seen in Fig. 12, the remaining intensity of the emv-coupled vibrational modes is small; this confirms that they are only very weakly coupled to charge carriers which are not localized on the dimers. Interestingly, this is only true for the metallic samples with high Br content (85% and 90%). Once we approach the insulating side of the phase diagram (low Br concentration), a charge transfer only in a dimer does not ac-

count for all the intensity of the emv-coupled features anymore. These spectra are much closer to those proposed by the tetramer model,<sup>62</sup> indicating that once the interdimer excitations get localized they are also coupled to the totally symmetric vibrations of the BEDT-TTF molecule.

### E. Anisotropy of the spectra

One of the striking features of the  $\kappa$ -phase spectra is the anisotropy, which from first glance one would not expect of an orthorhombic unit cell<sup>63</sup> with two crystallographically identical dimers and an angle between the optical axes and the dimers close to  $45^\circ$ . This anisotropy involves the intradimer transition,<sup>64</sup> and above we showed that the cluster model gives a good explanation for the anisotropy in the vibrational features.

It should be noted that the distance between the dimers is different in  $a$  and  $c$  directions, with some preference along the  $a$  axis, as depicted in Fig. 1. In addition, the molecules are not standing upright on the  $(ac)$  plane, but considerably tilted in the  $a$  direction (in an alternating fashion in such a way that adjacent layers form a herringbone pattern).<sup>57</sup> The higher reflectivity observed in the  $E||a$  polarization in these compounds suggests that a projection of the dipole moment for all the electronic transitions onto this axis is higher.

An alternative explanation for the difference in position and intensity of the intradimer charge-transfer band  $L_{\text{dimer}}$  observed parallel to  $a$  and  $c$  axes might be along the reasoning of the so-called Davydov splitting. In general, when the unit cell possesses a center of symmetry and there are two identical molecules in the cell, a Davydov splitting of the intramolecular electronic transitions between the upper molecular orbitals (intramolecular excitons, Frenkel excitons) is observed.<sup>65</sup> Because of this, instead of one absorption band, two bands are present in the spectra. They are distinct in position and intensity, and they are expected for the electric field polarized parallel to the symmetry axes of the unit cell. In the present case of the  $\kappa$  salts, the dimers are taken as the principal unit, i.e., a “big molecule” with one hole and a spin residing on it. We regard the intradimer transition as a transition of the charge carriers localized on dimers; in the first approximation, they are not involved in the metallic conductivity, as was shown in Sec. IV D. Thus, the anisotropy of the intradimer transition can be considered as a sort of Davydov splitting of the intradimer excitation.

It should be noted that the dimerization splits the conduction band, and here we discuss the interaction of the completely occupied portion. In other words, the Davydov-like splitting explains the anisotropy of the localized intradimer transition but does not include the itinerant conduction electrons. The itinerant electrons cause some screening, but in these bad metals the carrier concentration of  $10^{21}$   $\text{cm}^{-3}$  is considerably low. We consider excitonic effects possible even in the most metallic 85% and 90% Br compounds because only a quarter of the spectral weight is found in the Drude peak; the rest forms the intradimer transition or a transition between the Hubbard bands. The screening effect in the metallic compounds explains why the band of the intradimer transition becomes broader and less pronounced for

the more metallic compounds  $x=0.85\%$  and  $90\%$  and is stronger and well shaped for the compounds with lower Br concentration.

Due to the strong coupling of the electronic transition and intramolecular vibrations, these charge excitations may, in fact, form a charge-transfer vibronic exciton.<sup>66</sup> The electronic spectrum exhibits two distinct bands for the two polarizations parallel to the symmetry axes of the unit cell. Indeed, the less symmetrical (monoclinic)  $\kappa$ -(BEDT-TTF)<sub>2</sub>Hg(SCN)<sub>4</sub>X ( $X=\text{Cl, Br}$ ) lack the center of symmetry; consequently, their spectra<sup>67</sup> show less anisotropy than those of the presented orthorhombic compounds.

#### F. Allocating the transition between the Hubbard bands

From the analysis presented above, we conclude that the lower-frequency contribution  $L_{\text{Hubbard}}$  to the midinfrared band originates from excitations across the Mott-Hubbard gap, which allows us to determine the effective Coulomb repulsion  $U_{\text{eff}}$  to be approximately  $2200\text{ cm}^{-1}$ . This assignment is supported by comparing our data to the spectra of the superconductor  $\kappa$ -(BEDT-TSeF)<sub>4</sub>Hg<sub>2.89</sub>Br<sub>8</sub>. The replacement of the four inner sulfur atoms with selenium reduces the on-site Coulomb repulsion but increases the transfer integrals to neighboring molecules. Therefore, the BEDT-TSeF-based analogs are much closer to the normal metallic state; the contributions of itinerant and localized charge carriers are well separated in the optical spectra. It has clearly been observed<sup>50</sup> that with decreasing temperatures the contribution of the electrons in the conduction band (Drude peak and transitions between Hubbard bands) shifts to lower frequencies while there is a blueshift of the excitations of the localized charge carriers, similar to the metallic compounds studied in this work.

Calculations by Merino and McKenzie<sup>68</sup> reveal that in strongly correlated metals the coupling between electrons and phonons leads to a nonmonotonic temperature dependence of the vibrational modes near the coherence temperature  $T_{\text{coh}}$ . The shift is most pronounced (up to 5%) for phonons in the energy range comparable to  $U_{\text{eff}}/2$  and becomes weaker for larger or smaller frequencies. Raman measurements perfectly agree with these predictions.<sup>69</sup> Evidently, the situation is more complicated for infrared data, as the vibrations are activated only by emv coupling and influence in frequency and intensity by the charge excitations within the dimers. Nevertheless, this electron-phonon coupling might be an explanation for a softening of  $\nu_4(A_g)$  and  $\nu_6(A_g)$  below  $T_{\text{coh}} \approx 50\text{ K}$  for the compounds  $\kappa$ -(BEDT-

TTF)<sub>2</sub>Cu[N(CN)<sub>2</sub>]Br<sub>x</sub>Cl<sub>1-x</sub>, with  $x=0\%$  and  $40\%$  where the electronic correlations  $U/t$  are strongest. A close inspection of Figs. 5, 7, and 10 reveals that the higher-frequency mode  $\nu_{45}(B_{2u})$  exhibits a similar behavior for the insulating samples with low Br content, but weaker, while no change is observed for the far-infrared vibration  $\nu_{13}(A_g)$  around 50 K. This also suggests that the effective Coulomb repulsion  $U_{\text{eff}}$  is of the order of  $2000\text{--}2500\text{ cm}^{-1}$ .

#### V. CONCLUSION

Our comprehensive analysis of the temperature- and Br-concentration dependence of midinfrared and emv-coupled features in  $\kappa$ -(BEDT-TTF)<sub>2</sub>Cu[N(CN)<sub>2</sub>]Br<sub>x</sub>Cl<sub>1-x</sub> allows us to distinguish two contributions in the midinfrared part of the spectra. This interpretation is supported by the calculations which describe a charge transfer in a dimer and its coupling to the totally symmetric vibrations of the BEDT-TTF molecule. The higher-frequency  $L_{\text{dimer}}$  band ( $3300\text{ cm}^{-1}$  for the polarization  $E\parallel c$  and presumably around  $2900\text{ cm}^{-1}$  for  $E\parallel a$ ) originates from the charge transfer between the BEDT-TTF molecules in dimers. This charge transfer within the dimers is coupled to the intramolecular vibrations of BEDT-TTF and is responsible for the major part of the emv-coupled feature intensity for the metallic compounds, while in the insulating materials the lower-frequency contribution is presumably also coupled with vibrations. The lower-frequency contribution to the midinfrared band  $L_{\text{Hubbard}}$  located at  $2200\text{ cm}^{-1}$  is isotropic and assigned to the transition between two Hubbard bands which form due to strong electronic correlations. In Paper II (Ref. 27), the dynamical properties of the itinerant charge carriers will be analyzed and discussed in detail, including extensive calculations by the dynamical mean-field theory.

#### ACKNOWLEDGMENTS

The authors are grateful to Alain Barreau for help with the microscopic characterization of the sample concentrations. Belal Salameh performed the dc measurements. They acknowledge helpful discussions with Jaime Merino and Ross McKenzie, who initiated the study many years ago, and A. Girlando, M. Masino, A. Painelli, and V. S. Vikhnin. B.P., V.S., and R.V. thank V. Yartsev for useful discussions and the algorithm of calculations by a cluster model. The project was partially supported by the Deutsche Forschungsgemeinschaft (DFG). The authors from Ioffe Institute acknowledge the grant ‘‘Leading Scientific Schools’’ (NSh-5596.2006.2.). N.D. is grateful to the Alexander von Humboldt Foundation for its continuous support.

\*dressel@pi1.physik.uni-stuttgart.de

<sup>1</sup>D. Jérôme, in *Organic Conductors*, edited by J.-P. Farges (Dekker, New York, 1994), p. 405.

<sup>2</sup>T. Ishiguro, K. Yamaji, and G. Saito, *Organic Superconductors*, 2nd ed. (Springer-Verlag, Berlin, 1998).

<sup>3</sup>R. H. McKenzie, *Science* **278**, 821 (1997).

<sup>4</sup>H. Seo C. Hotta, and H. Fukuyama, *Chem. Rev. (Washington, D.C.)* **104**, 5005 (2004).

<sup>5</sup>M. Dressel and N. Drichko, *Chem. Rev. (Washington, D.C.)* **104**, 5689 (2004).

<sup>6</sup>T. Mori, H. Mori, and S. Tanaka, *Bull. Chem. Soc. Jpn.* **72**, 179 (1999).

- <sup>7</sup>By now, the observations are not completely understood: The coupling between the layers is certainly crucial; however, simple volume effects cannot explain this behavior.
- <sup>8</sup>A. Georges, G. Kotliar, W. Krauth, and M. J. Rozenberg, *Rev. Mod. Phys.* **68**, 13 (1996).
- <sup>9</sup>J. Merino and R. H. McKenzie, *Phys. Rev. B* **61**, 7996 (2000).
- <sup>10</sup>M. Lang and J. Müller, in *The Physics of Superconductors*, edited by K. H. Bennemann and J. B. Ketterson (Springer-Verlag, Berlin, 2004), Vol. 2, p. 453.
- <sup>11</sup>K. Miyagawa, A. Kawamoto, and K. Kanoda, *Phys. Rev. Lett.* **89**, 017003 (2002).
- <sup>12</sup>S. Lefebvre, P. Wzietek, S. Brown, C. Bourbonnais, D. Jérôme, C. Mezière, M. Fourmigué, and P. Batail, *Phys. Rev. Lett.* **85**, 5420 (2000).
- <sup>13</sup>P. Limelette, P. Wzietek, S. Florens, A. Georges, T. A. Costi, C. Pasquier, D. Jerome, C. Meziere, and P. Batail, *Phys. Rev. Lett.* **91**, 016401 (2003).
- <sup>14</sup>F. Kagawa, T. Itou, K. Miyagawa, and K. Kanoda, *Phys. Rev. B* **69**, 064511 (2004); *Phys. Rev. Lett.* **93**, 127001 (2004); F. Kagawa, K. Miyagawa, and K. Kanoda, *Nature (London)* **436**, 534 (2005).
- <sup>15</sup>J. E. Eldridge, K. Kornelsen, H. H. Wang, J. M. Williams, A. V. D. Crouch, and D. M. Watkins, *Solid State Commun.* **79**, 583 (1991).
- <sup>16</sup>M. Tamura, H. Tajima, K. Yakushi, H. Kuroda, A. Kobayashi, R. Kato, and H. Kobayashi, *J. Phys. Soc. Jpn.* **60**, 3861 (1991).
- <sup>17</sup>K. Kornelsen, J. E. Eldridge, H. H. Wang, H. A. Charlier, and J. M. Williams, *Solid State Commun.* **81**, 343 (1992).
- <sup>18</sup>J. E. Eldridge, Y. Xie, H. H. Wang, J. M. Williams, A. M. Kini, and J. A. Schlueter, *Spectrochim. Acta, Part A* **52**, 45 (1996); *Mol. Cryst. Liq. Cryst. Sci. Technol., Sect. A* **284**, 97 (1996).
- <sup>19</sup>R. M. Vlasova, O. O. Drozdova, V. N. Semkin, N. D. Kushch, and E. B. Yagubskii, *Phys. Solid State* **38**, 481 (1996).
- <sup>20</sup>J. J. McGuire, T. Rõdm, A. Pronin, T. Timusk, J. A. Schlueter, M. E. Kelly, and A. M. Kini, *Phys. Rev. B* **64**, 094503 (2001).
- <sup>21</sup>T. Sasaki, I. Ito, N. Yoneyama, N. Kobayashi, N. Hanasaki, H. Tajima, T. Ito, and Y. Iwasa, *Phys. Rev. B* **69**, 064508 (2004).
- <sup>22</sup>The optical study of an alloy  $\kappa$ -(BEDT-TTF)<sub>2</sub>Cu[N(CN)<sub>2</sub>]Br<sub>0.5</sub>Cl<sub>0.5</sub> was performed in midinfrared and could not give any information about the presence or absence of a Drude peak.
- <sup>23</sup>R. M. Vlasova, O. O. Drozdova, V. N. Semkin, N. D. Kushch, and E. B. Yagubskii, *Phys. Solid State* **35**, 408 (1993).
- <sup>24</sup>O. O. Drozdova, V. N. Semkin, R. M. Vlasova, N. D. Kushch, and E. B. Yagubskii, *Synth. Met.* **64**, 17 (1994).
- <sup>25</sup>B. V. Petrov, V. N. Semkin, R. M. Vlasova, V. M. Yartsev, N. D. Kushch, and A. Graja, in *Molecular Low-Dimensional and Nanostructured Materials for Advanced Applications*, edited by A. Graja *et al.* (Kluwer Academic, Dordrecht, 2002), p. 259.
- <sup>26</sup>K. D. Troung, B. Danilovic, D. Achkir, S. Jandl, and M. Poirier, *Synth. Met.* **85**, 1577 (1997).
- <sup>27</sup>M. Dumm, D. Faltermeier, N. Drichko, M. Dressel, C. Meziere, P. Batail, J. Merino, and R. McKenzie (unpublished).
- <sup>28</sup>D. Schweitzer (private communication).
- <sup>29</sup>The small size of the crystals limited our possibility of low-frequency measurements. In the case of the  $x=40\%$  sample, the crystal was so tiny that the measurements in the far-infrared (FIR) range were only possible without a polarizer due to the weak signal. Since the anisotropy of the spectra in the FIR range is low, it was possible to use the data for both polarizations.
- <sup>30</sup>The pure compound  $\kappa$ -(BEDT-TTF)<sub>2</sub>Cu[N(CN)<sub>2</sub>]Cl, follows the rise in  $\rho(T)$  down to about 30 K. At lower temperatures, the resistivity levels off at a value of approximately  $10^3 \Omega \text{ cm}$  and even shows a slight drop around  $T=10 \text{ K}$ . This behavior is well documented in literature (Refs. 31–33) and associated with traces of superconductivity induced by internal stress or surface effects. Similar effects are seen in samples with very low Br content  $x=15\%$  (Ref. 34).
- <sup>31</sup>J. M. Williams *et al.*, *Inorg. Chem.* **29**, 3271 (1990); H. H. Wang *et al.*, *Synth. Met.* **41–43**, 1983 (1991); M. Dressel, G. Grüner, K. D. Calson, H. H. Wang, and J. M. Williams, *ibid.* **70**, 927 (1995).
- <sup>32</sup>H. Ito, T. Ishiguro, M. Kubota, and G. Saito, *J. Phys. Soc. Jpn.* **65**, 2987 (1996).
- <sup>33</sup>H. Kobayashi, A. Miyamoto, T. Naito, R. Kato, A. Kobayashi, and J. M. Williams, *Chem. Lett.* **1991**, 1997 (1991).
- <sup>34</sup>V. A. Bondarenko, Yu. V. Sushko, V. I. Barchuk, V. S. Yefanov, V. V. Dyakin, M. A. Tanatar, N. D. Kushch, and E. B. Yagubskii, *Synth. Met.* **56**, 2386 (1993); Yu. V. Sushko, K. Andres, N. D. Kushch, and E. B. Yagubskii, *Solid State Commun.* **87**, 589 (1993); Yu. V. Sushko, T. Ishiguro, K. Andres, S. Horiuchi, G. Saito, N. D. Kushch, and E. B. Yagubskii, *J. Supercond.* **7**, 937 (1994); H. Posselt, H. Müller, K. Andres, Yu. V. Sushko, and G. Saito, *Synth. Met.* **70**, 917 (1995).
- <sup>35</sup>C. C. Homes, M. Reedyk, D. A. Cradles, and T. Timusk, *Appl. Opt.* **32**, 2976 (1993).
- <sup>36</sup>M. Dressel and G. Grüner, *Electrodynamics of Solids* (Cambridge University Press, Cambridge, 2002).
- <sup>37</sup>K. Kornelsen, J. E. Eldridge, H. H. Wang, and J. M. Williams, *Phys. Rev. B* **44**, 5235 (1991).
- <sup>38</sup>T. Sugano, H. Hayashi, M. Kinoshita, and K. Nishikida, *Phys. Rev. B* **39**, 11387 (1989).
- <sup>39</sup>M. J. Rozenberg, G. Kotliar, H. Kajueter, G. A. Thomas, D. H. Rapkine, J. M. Honig, and P. Metcalf, *Phys. Rev. Lett.* **75**, 105 (1995); M. J. Rozenberg, G. Kotliar, and H. Kajueter, *Phys. Rev. B* **54**, 8452 (1996).
- <sup>40</sup>R. H. McKenzie, *Comments Condens. Matter Phys.* **18**, 309 (1998).
- <sup>41</sup>D. Jung, M. Evain, J. J. Novoa, M. H. Whangbo, M. A. Beno, A. M. Kini, A. J. Schultz, J. M. Williams, and P. J. Nigrey, *Inorg. Chem.* **28**, 4516 (1989).
- <sup>42</sup>U. Geiser *et al.*, *Physica C* **74**, 475 (1991).
- <sup>43</sup>H. Kino and H. Fukuyama, *J. Phys. Soc. Jpn.* **64**, 2726 (1995); **64**, 4523 (1995); **65**, 2158 (1996).
- <sup>44</sup>K. Kanoda, *Hyperfine Interact.* **104**, 235 (1997).
- <sup>45</sup>A. Fortunelli and A. Painelli, *Phys. Rev. B* **55**, 16088 (1997).
- <sup>46</sup>By comparing the effects of “chemical” and hydrostatic pressure, Mori *et al.* (Ref. 6) point out that the application of the hydrostatic pressure (but also thermal contraction) to the Cl compound reduces the  $b1/p$  ratio, leading to a less correlated state.
- <sup>47</sup>M. Meneghetti, *Phys. Rev. B* **44**, 8554 (1991).
- <sup>48</sup>G. Visentini, M. Masino, C. Bellitto, and A. Girlando, *Phys. Rev. B* **58**, 9460 (1998).
- <sup>49</sup>V. M. Yartsev, O. O. Drozdova, V. N. Semkin, and R. M. Vlasova, *J. Phys. I* **6**, 1673 (1996); V. M. Yartsev, in *Materials and Measurements in Molecular Electronics*, edited by K. Kajimura and S. Kanoda (Springer-Verlag, Berlin, 1996), p. 189; V. M. Yartsev and A. Graja, *Int. J. Mod. Phys. B* **12**, 1643 (1998).
- <sup>50</sup>N. Drichko, B. Petrov, V. N. Semkin, R. M. Vlasova, O. A. Bogdanova, E. I. Zhilyaeva, R. N. Lyuboskaya, I. Olejniczak, H.

- Kobayashi, and A. Kobayashi, *J. Phys. IV* **114**, 305 (2004); R. M. Vlasova, N. V. Drichko, B. V. Petrov, V. N. Semkin, E. I. Zhilyaeva, R. N. Lyuboskaya, I. Olejniczak, A. Kobayashi, and H. Kobayashi, *Phys. Solid State* **46**, 1985 (2004).
- <sup>51</sup>J. E. Eldridge, C. C. Homes, H. H. Wang, A. M. Kini, and J. M. Williams, *Spectrochim. Acta, Part A* **51**, 947 (1995).
- <sup>52</sup>J. E. Eldridge, Y. Xie, Y. Lin, C. C. Homes, H. H. Wang, J. M. Williams, A. M. Kini, and J. A. Schlueter, *Spectrochim. Acta, Part A* **53**, 565 (1997).
- <sup>53</sup>Previously, the assignment of the modes was done assuming  $D_{2h}$  symmetry of the BEDT-TTF molecule (plane BEDT-TTF molecule) (Refs. 5, 17, 18, 51, 52, and 54). By now, the general agreement is that the molecules in  $\kappa$ -(BEDT-TTF)<sub>2</sub>Cu(NCS)<sub>2</sub> only have  $D_2$  due to the twisted ethylene groups (Refs. 55–57) leading to 19  $A_1$  totally symmetric modes. For the  $\kappa$ -(BEDT-TTF)<sub>2</sub>Cu[N(CN)<sub>2</sub>]Br and  $\kappa$ -(BEDT-TTF)<sub>2</sub>Cu[N(CN)<sub>2</sub>]Cl family, the molecules are eclipsed and exhibit only  $C_{2h}$  symmetry, as recently pointed out in Ref. 58.
- <sup>54</sup>M. E. Kozlov, P. I. Pokhodnia, and A. A. Yurchenko, *Spectrochim. Acta, Part A* **43**, 323 (1987); **45**, 437 (1989).
- <sup>55</sup>M. Meneghetti, R. Bozio, and C. Pecile, *J. Phys. (France)* **47**, 1377 (1986); M. Meneghetti, R. Bozio, and C. Pecile, *Synth. Met.* **19**, 143 (1987).
- <sup>56</sup>A. Girlando, M. Masino, A. Brillante, R. G. Della Valle, and E. Venuti, *Horizons in Superconductivity Research* (Nova Science, New York, 2004).
- <sup>57</sup>J. M. Williams, J. R. Ferraro, R. J. Thorn, K. D. Carlson, U. Geiser, H. H. Wang, A. M. Kini, and M. H. Whangbo, *Organic Superconductors* (Prentice-Hall, Englewood Cliffs, NJ, 1992).
- <sup>58</sup>R. Wesolowski, J. T. Haraldsen, J. Cao, J. L. Musfeldt, I. Olejniczak, J. Choi, Y. J. Wang, and J. A. Schlueter, *Phys. Rev. B* **71**, 214514 (2005).
- <sup>59</sup>Note that in the literature, the upper peak is commonly listed as the  $\nu_4$  frequency.
- <sup>60</sup>M. J. Rice, *Phys. Rev. Lett.* **37**, 36 (1976).
- <sup>61</sup>P. Delhaes and V. M. Yartsev, *Advances in Spectroscopy*, edited by R. J. H. Clark and R. E. Hester (Wiley, New York, 1993), Vol. 22, p. 199; V. M. Yartsev, O. Fichet, J.-P. Borgion, and P. Delhaes, *J. Phys. II* **3**, 647 (1993).
- <sup>62</sup>R. M. Vlasova, S. Ya. Priev, V. N. Semkin, R. N. Lyuboskaya, E. I. Zhilyaeva, E. B. Yagubskii, and V. M. Yarsev, *Synth. Met.* **48**, 129 (1992).
- <sup>63</sup>The dihedral angle is about 92°, which makes the charge transfer between the dimer contribute more strongly in the  $c$  direction.
- <sup>64</sup>If there were two different dimers, then we would expect the two optical axes parallel to these dipole vectors, i.e., approximately 45° to the crystallographic axes.
- <sup>65</sup>A. S. Davydov, *Theory of Molecular Excitons* (Plenum, New York, 1971).
- <sup>66</sup>V. S. Vikhnin, *Solid State Commun.* **127**, 283 (2003); *Phys. Solid State* **47**, 1490 (2005).
- <sup>67</sup>R. M. Vlasova, N. V. Drichko, O. O. Drozdova, and R. N. Lyubovskaya, *Phys. Solid State* **39**, 1165 (1997).
- <sup>68</sup>J. Merino and R. H. McKenzie, *Phys. Rev. B* **62**, 16442 (2000).
- <sup>69</sup>Y. Lin, J. E. Eldridge, H. H. Wang, A. M. Kini, M. E. Kelly, J. M. Williams, and J. A. Schlueter, *Phys. Rev. B* **58**, R599 (1998).